

LDP: Language-driven Dual-Pixel Image Defocus Deblurring Network

Hao Yang¹, Liyuan Pan^{1, †},

¹Beijing Institute of Technology

{hao.yang, liyuan.pan}@bit.edu.cn,

Yan Yang², and Miaomiao Liu²

² The Australian National University

{yan.yang, miaomiao.liu}@anu.edu.au

Abstract

Recovering sharp images from dual-pixel (DP) pairs with disparity-dependent blur is a challenging task. Existing blur map-based deblurring methods have demonstrated promising results. In this paper, we propose, to the best of our knowledge, the first framework to introduce the contrastive language-image pre-training framework (CLIP) to achieve accurate blur map estimation from DP pairs unsupervisedly. To this end, we first carefully design text prompts to enable CLIP to understand blur-related geometric prior knowledge from the DP pair. Then, we propose a format to input stereo DP pair to the CLIP without any fine-tuning, where the CLIP is pre-trained on monocular images. Given the estimated blur map, we introduce a blur-prior attention block, a blur-weighting loss and a blur-aware loss to recover the all-in-focus image. Our method achieves state-of-the-art performance in extensive experiments.

1. Introduction

Defocus deblurring from a single image is an ill-posed problem [18]. Compared to methods that restore an all-in-focus image directly [2, 3], blur map-based deblurring methods have demonstrated promising results [10, 14]. To simplify the blur removal process, several works [19, 12, 20] have utilized recent innovative dual-pixel (DP) sensors to estimate blur maps, since the DP sensor captures a two-view image pair (a DP pair) in a single shot. The DP pair can be treated as images from a two-sample light field camera or a stereo system with a tiny baseline, which is beneficial for disparity estimation [15, 2]. Based on the DP image pair formation process, the disparity is geometrically related to the blur map, i.e., the amount of defocus blur proportional to disparity magnitudes [7].

For estimating the blur map (defocus map or disparity map), previous works either require extra data [14, 1], such as synthetic data, for supervision signals, or pre-calibrated

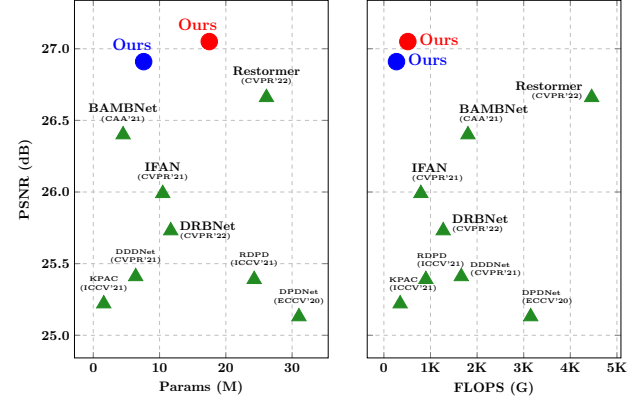


Figure 1: Comparison overview. We present the Parameters (M) vs. PSNR (dB) and FLOPS (G) vs. PSNR (dB). We use the **blue cycle** and **red cycle** to respectively denote our small and large models. The **green triangles** are past state-of-the-art methods, and each of them is annotated with the method name, publisher, and publication year. Best viewed in colors.

blur kernels [19]. To avoid using extra information, several works explored unsupervised blur map estimation frameworks [10, 12]. Lee *et al.* [10] implicitly estimate the disparity of the left/right views using a spatial transformer, yet only in feature space. Liang *et al.* [12] train an end-to-end network to estimate a four-layer defocus map by a four-branch network and then employ another four-branch network for deblurring. However, its fixed network branches and preset hyperparameters limited the potential of the estimation accuracy of the blur map.

Recently, the contrastive language-image pre-training framework (CLIP) [16] has accomplished extraordinary success for vision tasks, such as semantic segmentation, object detection and 3D point cloud understanding [17, 22]. Therefore, a question naturally arises, *can we avoid the cost of collecting data and model designing, to estimate the blur map unsupervisedly by using CLIP?* Unfortunately, using semantic knowledge from CLIP to handle low-level vision tasks has not been explored yet.

In this paper, for the first time, we explore the relationship between language and blur map estimation by applying

[†] Corresponding author.

CLIP. Note that CLIP is trained to match a monocular image with its corresponding language descriptions. Thus, CLIP requires the monocular image and the text to be encoded, respectively. Given a blurred image, it is intuitive to match it with a corresponding text [A blurry image.], which allows the language model to find the blur regions in an image. However, it is hard to quantize the blur level of an image without knowing its associated latent sharp one. Additionally, CLIP finds it challenging to simultaneously explore stereo DP pairs with left/right view images. To address these issues, we propose to explore the DP pair and propose a new image and text format to better capture the blurs in the image (Fig. 1).

Based on the DP pair formation, the detectable differences (disparities) in the left/right views directly correlate with the amount of defocus blurs. In other words, there is no disparity between left/right views for each pixel in the sharp regions. Hence, we can measure the difference between the left and right views, which can be quantized and treated as a cue for a blur map estimation. Inspired by these properties, we propose to create a new image from the DP pair and *translate* the description about the ‘blurriness’ of the image to measure the ‘symmetry’ of the newly formed image. The freshly designed image-text format allows the CLIP to estimate the blur map easily (see Sec. 3.1).

Given the estimated blur map, we then restore the all-in-focus image from the DP pair. By observing that the attention map of the self-attention mechanism [6] can be used in the dynamic DP deblurring process (Fig. 5), we introduce a blur prior attention (BPA) that modulates the attention map with the estimated blur map which provides prior knowledge of deblurring kernels (see Sec. 3.2).

To regulate the restoration, we specifically design two losses that are based on CLIP. Considering the network should focus more on heavily blurred regions, we propose a blur-weighting loss that imposes an adaptive penalty proportional to the blur degrees provided by the estimated blur map from CLIP. Then, to guarantee the restored image is sharp, we use CLIP to re-check the restored image and formulate a blur-aware loss (see Sec. 3.3).

Our contributions are summarised as follows:

- We propose a **Language-driven DP (LDP)** defocus deblurring framework, by exploring the potential of CLIP in the low-level vision task.
- We design an image-text format for blur map estimation based on the geometric relationship between the blur and disparity of the DP pair.
- We propose a blur prior attention (BPA) block, a blur-weighting loss, and a blur-aware loss to encourage sharp restorations of the DP pair.

We evaluate the proposed framework on extensive standard benchmark datasets. We show that our LDP outperforms state-of-the-art (SOTA) methods in image restoration

performance (refer to Fig. 1 for an overview comparison). Our codes and models will be released to facilitate reproducible research.

2. Related Work

DP Defocus Deblurring. DP-based deblurring methods can be divided into single- and multi-task based manners. For single task-based deblurring [2, 3, 1], methods apply different kernels at different regions of the DP pair to handle the spatially varying defocus deblur. This can usually be achieved by using parallel atrous convolutions [18], attention mechanisms [21], or deformable convolutions [11]. For multi-task deblurring methods, the blur/defocus/disparity map is auxiliarily estimated for benefiting DP defocus deblurring. Pan *et al.* [14] and Xin *et al.* [19] use the estimated DP disparity to regularise the restoration through re-blurring; however, with extra data or pre-calibrate kernel. Several works explored unsupervised defocus map (or disparity) estimation. Lee *et al.* [10] estimate defocus disparity only in feature space without explicitly showing a defocus map. Liang *et al.* [12] optimize a multi-channel defocus map based on [15]. However, hyperparameters, such as the defocus threshold and the number of channels, are preset, limiting blur map estimation accuracy. Unlike past works, by transferring the blur-related geometric prior knowledge into semantic prompts, we unsupervisedly estimate the blur map from CLIP to benefit defocus deblurring.

Language-driven Vision Common objectives in visual-language learning are aligning the text with a paired image in the embedding space [16]. The CLIP, one of the milestone achievement in the area, demonstrate that language-independent computer vision tasks can be substantially benefited from visual-language learning, by achieving SOTA zero-short classification performance in the ImageNet-1K benchmark [5]. Successive works have extended the zero-short learning capability of CLIP to semantic segmentation [17], depth estimation [23], and point clouds [22]. However, none of the existing works explores the zero-short learning capability of CLIP in stereo/DP images. This paper proposes an approach to use the monocular image trained CLIP in zero-short blur map segmentation of DP image.

3. Method

Let us now introduce our language-driven dual-pixel image defocus deblurring framework. Given a defocus blurred DP pair (B_L, B_R), we aim to restore an all-in-focus image I , where B_L and B_R are the left and right view of a DP pair and $B_L, B_R, I \in \mathbb{R}^{h \times w \times 3}$. Here, h and w define the image height and width, respectively.

We first design a DP-aware prompt to adapt CLIP to output a blur map, $M \in \mathbb{R}^{h \times w \times 1}$, which quantizes disparity unsupervisedly between B_L and B_R . Then, we pro-

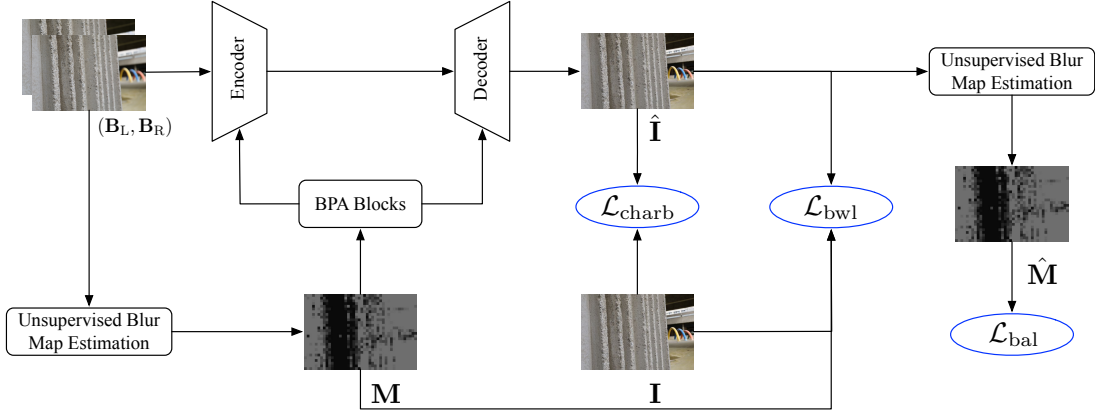


Figure 2: Method overview. Given a DP pair $(\mathbf{B}_L, \mathbf{B}_R)$, we first generate the blur map \mathbf{M} by using our unsupervised blur map estimation strategy which is based on the CLIP, and the DP-aware format is used. We then forward the DP pair $(\mathbf{B}_L, \mathbf{B}_R)$ to our deblurring backbone composed of an encoder and a decoder. Meanwhile, we have multiple BPA blocks, using the blur map \mathbf{M} as deblurring kernel prior to refine the intermediate backbone feature embeddings. In the following, we have the restoration $\hat{\mathbf{I}}$. The deblurring network is optimized with three losses, charbonnier loss $\mathcal{L}_{\text{charb}}$, blur weighting loss \mathcal{L}_{bwl} , and blur aware loss \mathcal{L}_{bal} . $\mathcal{L}_{\text{charb}}$ penalizes deviations from \mathbf{I} in the restoration $\hat{\mathbf{I}}$. \mathcal{L}_{bwl} and \mathcal{L}_{bal} regularize the restoration by imposing an adaptive penalty on the blurred regions of the DP pair; and leveraging unsupervised blur map estimation strategy to encourage the restoration to be sharp, i.e., the blur map $\hat{\mathbf{M}}$ for the restoration $\hat{\mathbf{I}}$ is zero value filled.

pose a BPA block based network which employs the blur map \mathbf{M} as deblurring priors to restore a sharp image $\hat{\mathbf{I}}$ from $(\mathbf{B}_L, \mathbf{B}_R)$. To regularize the restoration of $\hat{\mathbf{I}}$, a blur-weighting loss \mathcal{L}_{bwl} and a blur-aware loss \mathcal{L}_{bal} are also introduced that were underpinned by our unsupervised blur map estimation strategy. The overall framework is shown in Fig. 2. Details are presented below.

3.1. Unsupervised Blur Map Estimation

Preliminary. CLIP respectively embeds an image and a text description into a common semantic space of dimension c with an image encoder and a text encoder, obtaining image embedding $\mathbf{f} \in \mathbb{R}^c$ and text embedding $\mathbf{t} \in \mathbb{R}^c$. By optimizing a contrastive loss, the embeddings of the aligned image and text pair stay similar, i.e., maximizing the semantic similarity by $\max \text{sim}(\mathbf{f}, \mathbf{t})$, where $\text{sim}(\cdot, \cdot)$ is the cosine similarity metric. Meanwhile, the semantics of misaligned pairs are pushed away from each other, i.e., $\min \text{sim}(\mathbf{f}, \mathbf{t})$. With comprehensive training data, CLIP can be leveraged to align images with pre-defined prompt templates composed of open-world text descriptions for zero-shot learning [16].

For a DP pair, the disparity d for a pixel in the left view is defined by its location (i, j) and that of its corresponding pixel at (i, k) in the right view. In the literature, this DP disparity [15] is defined as

$$d = j - k = A(r(z)) \cdot B(z), \quad \mathbf{B}_L(i, j) = \mathbf{B}_R(i, k), \quad (1)$$

where $\mathbf{B}_L(i, j)$ and $\mathbf{B}_R(i, k)$ are the intensity of the two matching points, $r(\cdot)$ is a function of the radius of the circle of confusion, z is the point depth, and $A(r(z))$ and $B(z)$ are lens-dependent constants [14, 19, 3, 7].

Analysis. Leveraging the CLIP, zero-shot blur map estimation can be generally divided into three steps. *i) Image Encoding.* Considering the image encoder of the CLIP is trained with monocular RGB images, a function $\eta(\cdot, \cdot)$ is required to create a new monocular image from the DP image pair $(\mathbf{B}_L, \mathbf{B}_R)$. To obtain the dense embedding for the blur map estimation task, we follow [23] to pop out the final pooling layer from the image encoder, yielding an embedding matrix $\mathbf{F} \in \mathbb{R}^{h_s \times w_s \times c}$, where h_s and w_s are the height and width for embedding of the newly created image, respectively. Mathematically, we have

$$\mathbf{F} = \text{ImageEncoder}(\eta(\mathbf{B}_L, \mathbf{B}_R)). \quad (2)$$

where each pixel of \mathbf{F} has encoded the local semantic information for a corresponding region in $\eta(\mathbf{B}_L, \mathbf{B}_R)$. *ii) Text Encoding.* A text encoder is used to embed the semantics of a prompt p describing the blur into the text embedding,

$$\mathbf{t} = \text{TextEncoder}(p). \quad (3)$$

iii) Blur map estimation. Let $\mathbf{F}(i, j)$ be a c -dimensional embedding at position (i, j) of \mathbf{F} , $i \in \{1, \dots, h_s\}$, and $j \in \{1, \dots, w_s\}$. The embedding $\mathbf{F}(i, j)$ and the blur semantic-based text embedding \mathbf{t} are expected to be similar if the pixel at (i, j) is blurred. Therefore, the blur mask \mathbf{M}_F of $\eta(\mathbf{B}_L, \mathbf{B}_R)$ is obtained by

$$\mathbf{M}_F(i, j) = \sigma(\text{sim}(\mathbf{F}(i, j), \mathbf{t})). \quad (4)$$

Note, $\sigma(\cdot)$ normalizes the cosine similarity $\text{sim}(\cdot, \cdot)$ output to a probability space, to reflect the amount of blur at the position. Here, \mathbf{M}_F is sampled to have the same resolution of \mathbf{B}_L or \mathbf{B}_R , returning $\mathbf{M} \in \mathbb{R}^{h \times w \times 1}$.

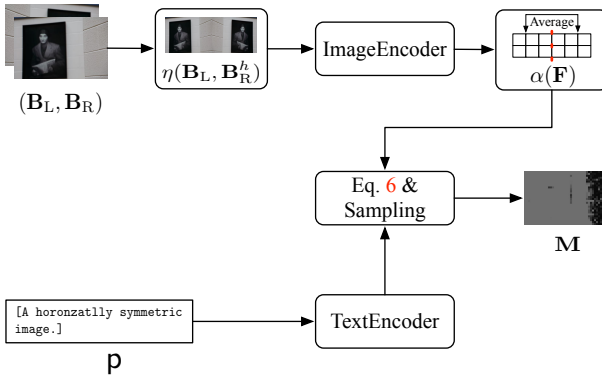


Figure 3: The pipeline of our DP-aware format for obtaining the blur map M . Given a DP pair (B_L, B_R) , the function $\eta(B_L, B_R^h)$ concatenates the left view B_L and with horizontally flipped right view B_R^h for obtaining the F from the CLIP image encoder. We then apply $\alpha(F)$ to averagely pool the feature map according to the transformation imposed on the input DP pair, resulting in a new feature embedding with the same aspect ratio of the input DP pair. Meanwhile, we set the prompts p to describe the symmetry of $\eta(B_L, B_R^h)$, obtaining text embedding t . We finally have the blur map M by computing Eq. 6 and performing sampling.

Overall, our explored formats of the prompt p (while adapting the function $\eta(\cdot, \cdot)$) enables the use of semantic knowledge from CLIP to generate the blur map M in an unsupervised manner. We describe the blur-aware, DP-aware, and ensembling formats below.

Blur-aware Format. An intuitive approach is setting a prompt p that describes the blur to query a blur map M , e.g., $p = [\text{A blurry image.}]$. The $\eta(\cdot, \cdot)$ is then defined to synthesize a center view of the DP pair by averaging the left view B_L and right view B_R , as the average of two sub-images is equivalent to the image captured by a regular sensor [15, 1]. However, the disparity information among the DP pair is neglected, resulting in a sub-optimal blur map. Refer to Fig. 4 for comparisons.

DP-aware Format. Considering disparity is proportional to the amount of blur exhibited in the DP view [2], guiding CLIP to understand the disparity exhibited between B_L and B_R can contribute for generating the mask M . We first formulate the disparity in the DP pair and then study the disparity-aware prompt and function $\eta(\cdot, \cdot)$ designing. Thus, we query degrees of displacement between the left and right view from the CLIP, without any fine-tuning, to obtain the blur map M .

Note that the CLIP is the vision-text alignment model trained with monocular image input. To extract the displacement between left/right views of the DP pair, we explore several input-prompt formats: i) Concatenating the left and right views horizontally, and prompting their difference, e.g., [The left and right of the image are different.]; ii) Prompting the horizontal symmetry between the left and right views, e.g., [A

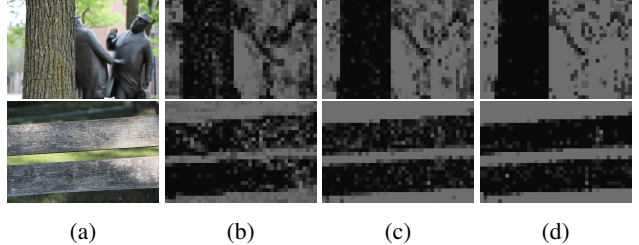


Figure 4: Blur map estimation. We show the left view of the DP image in (a), and blur maps obtained with blur-aware approach (b), DP-aware approach (c), and ensembling-based approach (d) in sequence (the darker, the sharper). For the ensembling-based approach, 8 prompts from blur-aware and DP-aware formats are used, and please refer to Tab. 4 for details.

horizontally symmetric image.] (Fig. 3).

Empirically, we achieve the best performance with the second prompt format. When describing the symmetry in the prompt p , we concatenate the left view B_L with a horizontally flipped right view $B_R^h = \text{Flip}(B_R)$ along the width axial in the $\eta(\cdot, \cdot)$. We then obtained image features $F = \text{ImageEncoder}(\eta(B_L, B_R^h))$. To transform F to the same aspect ratio of B_L and B_R , we use $\alpha(F)$ to average the corresponding pixel-wise features based on the transformation in $\eta(B_L, B_R^h)$. For $i \in \{1, \dots, h_w\}$ and $j \in \{1, \dots, \lfloor \frac{1}{2}w_s \rfloor\}$, we define

$$\alpha(F)(i, j) = \frac{1}{2}F(i, j) + \frac{1}{2}F(i, w_s - j). \quad (5)$$

Back to the left-hand side of Eq. 4, we have

$$M_F(i, j) = 1 - \sigma(\text{sim}(\alpha(F)(i, j), t)). \quad (6)$$

Here, t is the text embedding of the prompt describing symmetry. Note that the similarity is reversed when calculating the blur map, as the symmetric means sharp pixel, and therefore the ‘1’ exist in Eq. 6. Similarly, the M_F is sampled to the same resolution of the DP pair, returning M .

For this blur map estimation strategy, we conclude the lemma below,

Lemma 3.1. *A pixel is sharp if and only if it is horizontally symmetric in the left view and the horizontally flipped right view, otherwise, the pixel is blurred.*

Proof. Following Eq. (1), we have $B_L(i, j)$ being sharp, given $B_L(i, j) = \text{Flip}(B_R)(i, w_s - j)$. In other words, we have $\eta(B_L, B_R^h)(i, j) = \eta(B_L, B_R^h)(i, w_s - j)$, demonstrating the horizontal symmetry. Reversely, the horizontal symmetry breaks once the disparity/blur occurs. \square

Ensembling format. Considering the blur effect in the DP pair is disparity-aware, we obtain the mask from the blur-aware and DP-aware formats jointly (Fig. 3). Please refer to Tab. 4 for details of the designed 8 prompts from blur-aware and DP-aware formats.

3.2. Network

We train an encoder-decoder based deblurring network [4] for restoring the DP pair $(\mathbf{B}_L, \mathbf{B}_R)$ into a restoration $\hat{\mathbf{I}}$. A BPA block is proposed to interleave with the backbone network. It uses the obtained blur map \mathbf{M} as the blur kernel prior to refining the intermediate feature embeddings of $(\mathbf{B}_L, \mathbf{B}_R)$ in the backbone network on the fly.

Analysis. The self-attention mechanism is widely used in the defocus deblurring tasks [21]. We first briefly review it. Let $\mathbf{X} \in \mathbb{R}^{h_x \times w_x \times c_x}$ be the intermediate feature embedding of a blur image from the backbone, where h_x, w_x, c_x are height, width, and channel of the feature. The self-attention is input with query \mathbf{Q} , key \mathbf{K} , and value \mathbf{V} that are linear projected from \mathbf{X} , and then calculate an attention map between \mathbf{Q} and \mathbf{K} for adaptively aggregating \mathbf{V} . This process is defined as follows,

$$\mathbf{Q} = \mathbf{XW}_Q, \quad \mathbf{K} = \mathbf{XW}_K, \quad \mathbf{V} = \mathbf{XW}_V, \quad (7)$$

$$\text{Attention}(\mathbf{Q}, \mathbf{K}, \mathbf{V}) = \text{Softmax}(\mathbf{Q}\mathbf{K}^\top/\beta)\mathbf{V}, \quad (8)$$

where $\mathbf{W}_Q, \mathbf{W}_K, \mathbf{W}_V \in \mathbb{R}^{h_x \times w_x \times c_x}$ are learnable weight matrix, β is a normalization factor that is typically set to the square root of the latent dimension, and $\text{Softmax}(\mathbf{Q}\mathbf{K}^\top/\beta) \in \mathbb{R}^{(h_x \times w_x) \times (h_x \times w_x)}$ is known as the attention map.

In our DP deblurring task, we hypothesize that the attention map acts as an adaptive deblur kernel in the feature space. A simple experiment is conducted to verify our assumption in Fig. 5. In detail, we manually reset the attention map to the identity matrix in a pre-trained self-attention based DP deblurring network, and observe negligible restoration performance.

BPA Block. With the above verification, we are motivated to modulate the attention map by supplying the blur map \mathbf{M} , utilizing blur-related prior knowledge to additionally assign a $q \times q$ deblur kernel for each region in \mathbf{X} . This considers the nearby regions of each region for aggregating a sharp feature embedding. We re-write the Eq. 8 as

$$\text{Attention}(\mathbf{Q}, \mathbf{K}, \mathbf{V}) = \text{Softmax}(\mathbf{Q}\mathbf{K}^\top/\beta + \mathbf{O})\mathbf{V}, \quad (9)$$

$$\mathbf{O} = \text{Pad}(\text{FFN}_{\text{Conv}}(\sigma^{-1}(\mathbf{M}))), \quad (10)$$

where $\text{FFN}_{\text{Conv}}(\cdot)$ is a convolution-based feed forward layer that is used to learn a $q \times q$ deblur kernel for each region of \mathbf{X} from the unnormalized blur map $\sigma^{-1}(\mathbf{M})$, resulting in $\text{FFN}_{\text{Conv}}(\sigma^{-1}(\mathbf{M})) \in \mathbb{R}^{h_x \times w_x \times q^2}$. The $\text{Pad}(\cdot)$ function reshapes $\text{FFN}_{\text{Conv}}(\sigma^{-1}(\mathbf{M}))$ into $\mathbb{R}^{h_x \times w_x \times q \times q}$, and pads the reshaped $\text{FFN}_{\text{Conv}}(\sigma^{-1}(\mathbf{M}))$ to $\mathbb{R}^{(h_x \times w_x) \times (h_x \times w_x)}$, for shape alignment issue.

3.3. Network Training

We optimize our deblurring network with the widely used Charbonnier loss. Moreover, we propose a blur-aware

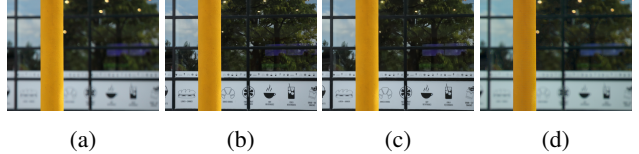


Figure 5: *Attention map evaluations.* We assume the attention matrix serves as deblurring kernels in the self-attention based deblurring network. (a) and (b) are the left view of the DP pair and the ground truth sharp image. The deblurred image is given in (c). When manually setting the attention map to an identity matrix, we have (d), exhibiting no deblurring effects, and verifying our assumption. Zoom in for better quality.

loss and a blur weighting loss to penalize the blurred regions in the restoration $\hat{\mathbf{I}}$.

Charbonnier loss. We encourage the restoration to close with the ground truth by using Charbonnier loss. We empirically set ε to 10^{-4} , and define:

$$\mathcal{L}_{\text{char}} = \sqrt{\|\mathbf{I}(i, j) - \hat{\mathbf{I}}(i, j)\|^2 + \varepsilon^2}. \quad (11)$$

Blur Weighting Loss. We impose an adaptive penalty on the blurred regions of the DP pair $(\mathbf{B}_L, \mathbf{B}_R)$, considering the degree of blur measured by CLIP. It encourages the network to focus on the restoration of heavily blurred regions. We first normalize the deviations between $\hat{\mathbf{I}}$ and \mathbf{I} by the deviations between $(\mathbf{B}_L, \mathbf{B}_R)$ and \mathbf{I} , and then re-use the blur map to select blurred regions residing in the DP pair.

$$\mathcal{L}_{\text{bwl}} = \frac{\|\mathbf{I}(i, j) - \hat{\mathbf{I}}(i, j)\|^2}{\|\mathbf{I}(i, j) - \frac{1}{2}(\mathbf{B}_L(i, j) + \mathbf{B}_R(i, j))\|^2} \cdot \mathbf{M}(i, j), \quad (12)$$

where we use the blur map \mathbf{M} (with soft logits) to reflect the blur levels detected by CLIP.

Blur-aware Loss. We encourage the $\hat{\mathbf{I}}$ to be sharp by leveraging the versatile knowledge contained in the CLIP. We generate the blur map $\hat{\mathbf{M}}$ by the blur-aware format for the restoration, and penalize the blur exhibited in $\hat{\mathbf{I}}$. Similar to \mathcal{L}_{bwl} , we use the unnormalized version of the blur map,

$$\mathcal{L}_{\text{bal}} = \hat{\mathbf{M}}(i, j). \quad (13)$$

This encourages the $\hat{\mathbf{M}}$ to be zero value filled, i.e., no blur exhibited in the restoration.

Total Loss. Our network is optimized under

$$\mathcal{L}_{\text{total}} = \frac{1}{|\Omega|} \sum_{(i, j) \in \Omega} (\mathcal{L}_{\text{char}} + \lambda_1 \mathcal{L}_{\text{bal}} + \lambda_2 \mathcal{L}_{\text{bwl}}), \quad (14)$$

where $\frac{1}{|\Omega|}$ is a normalization factor determined by the image domain size $|\Omega|$, and λ_1 and λ_2 are hyperparameters to balance losses.

Table 1: Quantitative comparisons on the DPD-blur dataset [2] composed of 37 indoor and 39 outdoor scenes. We respectively color the best and the second-best performance in red and blue.

Method	Outdoor Scenes				Indoor Scenes				Average			
	PSNR \uparrow	SSIM \uparrow	MAE \downarrow	MSE_rel \downarrow	PSNR \uparrow	SSIM \uparrow	MAE \downarrow	MSE_rel \downarrow	PSNR \uparrow	SSIM \uparrow	MAE \downarrow	MSE_rel \downarrow
EBDB	25.77	0.772	0.040	0.051	21.25	0.599	0.058	0.086	23.45	0.683	0.049	0.067
DMENet	25.50	0.788	0.038	0.053	21.43	0.644	0.063	0.084	23.41	0.714	0.051	0.067
DPDNet	27.48	0.849	0.029	0.042	22.90	0.726	0.052	0.071	25.13	0.786	0.041	0.055
RDPD	28.10	0.843	0.027	0.039	22.82	0.704	0.053	0.072	25.39	0.772	0.040	0.053
DDDNet	27.57	0.833	0.030	0.041	23.28	0.708	0.050	0.068	25.36	0.768	0.041	0.054
IFAN	28.66	0.868	0.025	0.037	23.46	0.743	0.049	0.067	25.99	0.804	0.037	0.050
BAMBNet	28.60	0.872	0.026	0.037	24.30	0.772	0.045	0.060	26.40	0.821	0.036	0.047
DeepRFT	28.48	0.870	0.025	0.038	23.09	0.736	0.051	0.070	25.71	0.801	0.037	0.051
Restormer	29.48	0.895	0.023	0.034	23.97	0.773	0.047	0.063	26.66	0.833	0.035	0.046
Ours (Small)	29.55	0.893	0.021	0.033	24.38	0.773	0.043	0.065	26.91	0.831	0.032	0.045
Ours (Large)	29.67	0.896	0.020	0.032	24.57	0.786	0.037	0.059	27.05	0.839	0.029	0.044

Table 2: Quantitative comparisons on DDD-syn dataset.

Method	PSNR \uparrow	SSIM \uparrow	MAE \downarrow	MSE_rel \downarrow
EBDB	26.48	0.683	0.036	0.047
DMENet	30.14	0.939	0.017	0.031
DPDNet	31.45	0.926	0.016	0.027
RDPD	32.42	0.912	0.016	0.024
DDDNet	33.21	0.956	0.010	0.022
IFAN	34.18	0.929	0.012	0.020
BAMBNet	35.90	0.954	0.012	0.016
DeepRFT	36.52	0.952	0.010	0.015
Restormer	36.44	0.957	0.010	0.015
Ours (Small)	37.27	0.959	0.010	0.014
Ours (Large)	38.13	0.963	0.009	0.012

Table 3: Quantitative comparisons on RDPD dataset.

Method	PSNR \uparrow	SSIM \uparrow	MAE \downarrow	MSE_rel \downarrow
EBDB	24.23	0.637	0.031	0.054
DMENet	25.17	0.731	0.036	0.061
DPDNet	29.84	0.828	0.032	0.055
RDPD	31.09	0.861	0.025	0.028
DDDNet	30.14	0.840	0.016	0.031
IFAN	31.12	0.865	0.023	0.028
BAMBNet	31.78	0.867	0.016	0.026
DeepRFT	31.71	0.879	0.016	0.024
Restormer	32.27	0.871	0.016	0.024
Ours (Small)	32.98	0.895	0.014	0.022
Ours (Large)	33.25	0.899	0.013	0.021

4. Experiments and Analysis

Implementation Details. We implement our model under the PyTorch framework. We use the pre-trained and ViT-B/32 [6] architecture-based CLIP [16] for our blur map estimation strategy. We train the deblurring network in two stages for 6×10^6 steps in total with the Adam optimizer. In each stage, the learning rate is decayed from 2×10^{-4} to 10^{-6} by a cosine annealing strategy. In the first stage, we train the network for 5×10^6 steps, and only use the Charbonnier loss $\mathcal{L}_{\text{char}}$. In the second stage, the network is finetuned for 1×10^6 steps with $\mathcal{L}_{\text{total}}$, where we have $\lambda_1 = 10^{-1}$ and $\lambda_2 = 2 \times 10^{-1}$. More implementation details are given in our supplementary material.

Datasets. Our method is evaluated on three real-world DP defocus deblurring datasets, DPD-blur dataset [2] and DPD-disp dataset [15], and PixelDP dataset [19]. We follow [2] on the training and testing splits. For the DPD-disp dataset and PixelDP dataset, we use them for testing only, re-using the checkpoints trained from the DPD-blur dataset as they do not provide ground-truth (GT) data or with limited dataset size. Moreover, two synthetic datasets, DDD-syn [14] and RDPD [19], are also used for evaluations.

Evaluation Metrics. We use peak signal-to-noise ratio (PSNR), structural similarity (SSIM), mean absolute error (MAE), and relative mean squared error (MSE_rel) as our evaluation metrics.

Baseline Methods. We compare with SOTA DP defocus deblurring methods, i.e., EBDB [8], DMENet [9], DPDNet [2], RDPD [3], DDDNet [14], IFAN [10], BAMBNet [12], DeepRFT [13], and Restormer [21].

4.1. Comparisons with State-of-the-Art

Quantitative Comparison. We compare with the state-of-the-art methods on the DPD-blur, DDD-syn, and RDPD datasets in Tab. 1, Tab. 2, and Tab. 3, respectively. We train our model with small and large configurations, and details are given in our supplementary material. Our observations are as follows: i) With our model (Small), we achieve similar restoration results with Restormer, the second-best method, in all datasets. ii) When scaling to the large model, we consistently outperform all methods on all evaluation metrics. For example, our method and Restormer respectively achieve 27.05/26.66, 38.13/36.44, and 33.25/32.27 PSNR (dB) in the DPD-blur, DDD-syn, and RDPD datasets. Meanwhile, on a single RTX 3090 GPU, we remain to have

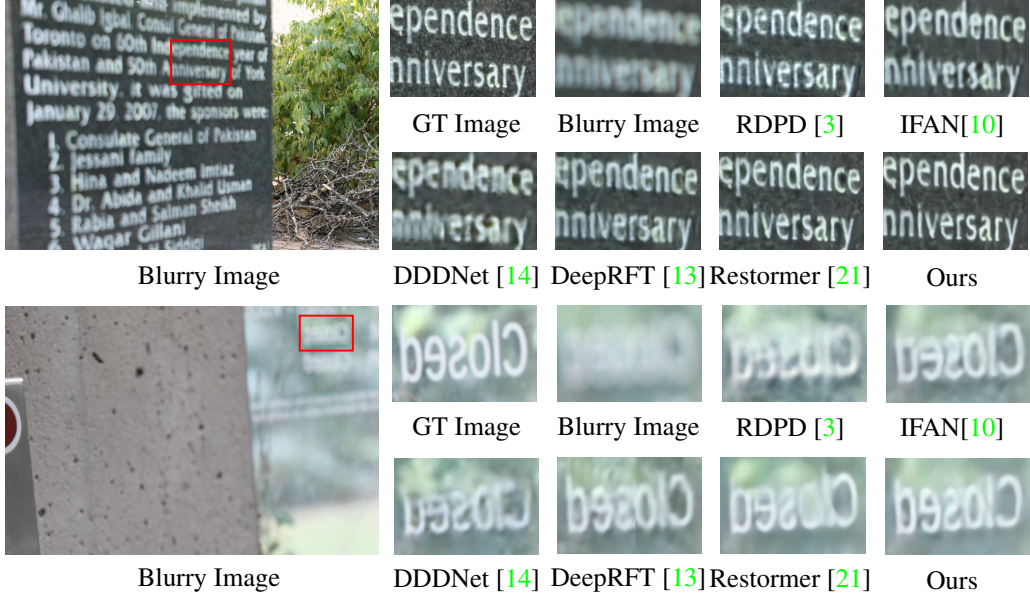


Figure 6: Qualitative comparison on the DPD-blur dataset [2]. We present the blurry image (\mathbf{B}_L) in the first column, and the ground truth (GT) image of regions residing in the red bounding box is shown in the second column. The cropped blurred image of the red bounding box regions is in the third column.

a lower Infer. time (considering the frozen parameters in CLIP) which is 0.137s, while Restormer takes 0.161s.

Qualitative Comparison. We compare with state-of-the-art methods on the DPD-blur dataset (Fig. 6). As shown, our method performs sharper and clearer restorations of edges and texts. To further demonstrate the benefits of using CLIP to generate the blur mask unsupervisedly in our approach, we provide an example in Fig. 7, which preserves sharp regions (e.g., text ‘York’) in the input blur image effectively compared to the second-best baseline.

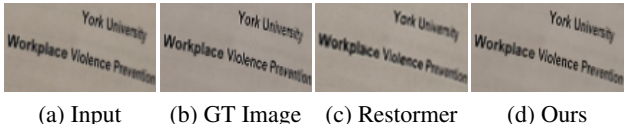


Figure 7: An example of the restoration results on the sharp region of the input DP image (left view).

4.2. Ablation Study

We study model architecture, blur map estimation, and losses in this section. All experiments are performed in the DPD-blur dataset.

Ablation of Model Architecture. We study the effective usage of blur map as prior knowledge for DP defocus deblurring (Tab. 6). To show the benefits of using blur maps for DP deblurring, we consider four baselines: i) NAFNet [4] that is our baseline architecture. ii) Concat concatenates the blur map with the DP pair before feeding to the model; iii) SA adds the past self-attention layer [6] to the model; iv) Concat+SA combines the Concat and SA settings. Our BPA block directly set the blur map as deblurring

kernel prior, and consistently outperforms all baseline settings. Compared to the second-best setting, Concat + SA, we have 0.13/0.002 higher PSNR (dB)/SSIM.

Ablation of Losses. We investigate the proposed blur weighting loss \mathcal{L}_{bwl} and blur-aware loss \mathcal{L}_{bal} (Tab. 7) with a baseline as the $\mathcal{L}_{\text{char}}$ setting. We first use \mathcal{L}_{bwl} and \mathcal{L}_{bal} to our baseline, NAFNet (i.e., not using our BPA block), that only uses $\mathcal{L}_{\text{char}}$, having 0.32 PSNR (dB) improvements. Secondly, we train our model (backbone + BPA block) with Charbonnier loss, resulting in 26.71/0.825 higher PSNR (dB)/SSIM. By using the \mathcal{L}_{bwl} or \mathcal{L}_{bal} , we respectively achieve 0.05/0.003 or 0.10/0.004 higher PSNR (dB)/SSIM. Combining all losses, we have the best restoration performance at 26.91/0.831 for PSNR (dB)/SSIM.

Ablation of Blur Map Estimation. We ablate with different prompts used to generate the blur map. The blur-aware and DP-aware prompts are presented in Tab. 4, and we show their impact on model performance with Tab. 5. We then ensemble the groups of blur-aware prompt and disparity-aware prompt individually (Ens.¹), leading to 26.80dB/0.829 and 26.84/0.830 PSNR (dB)/SSIM. By ensembling all prompts (Ens.²), we have 26.91/0.831 PSNR (dB)/SSIM, consistently outperforming other approaches of generating blur masks. More ablations and analyses of CLIP can be found in our supplementary material.

4.3. Discussion and Limitation

Discussion. The reader may wonder about the performance of our unsupervised blur map estimation strategy. Therefore, we perform two qualitative evaluations on the

Table 4: Prompts used for blur map estimation.

Blur-aware Prompt		DP-aware Prompt
p_1	[A blurry image.]	[A symmetrical image.]
p_2	[An obscured image.]	[A horizontally symmetrical image.]
p_3	[An out of focus image.]	[A left-right symmetrical image.]
p_4	[An image lacking sharpness.]	[A symmetrical image at the pixel level.]

Table 5: Restoration performance of our methods by using blur-aware or/and DP-aware prompts for blur map estimation. Ens.¹ denotes ensembling the group of blur-aware prompts and DP-aware prompts individually, and Ens.² ensembles all prompts.

	Blur-aware Prompt				DP-aware Prompt			
	PSNR \uparrow	SSIM \uparrow	MAE \downarrow	MSE $_{\text{rel}}\downarrow$	PSNR \uparrow	SSIM \uparrow	MAE \downarrow	MSE $_{\text{rel}}\downarrow$
p_1	26.83	0.829	0.033	0.045	26.82	0.830	0.033	0.046
p_2	26.81	0.829	0.033	0.046	26.83	0.830	0.032	0.046
p_3	26.75	0.828	0.034	0.046	26.82	0.830	0.033	0.046
p_4	26.77	0.829	0.033	0.046	26.85	0.830	0.032	0.045
Ens. ¹	26.80	0.829	0.033	0.046	26.84	0.830	0.032	0.046
Ens. ²	26.91	0.831	0.032	0.045	26.91	0.831	0.032	0.045

Table 6: Ablation of model architectures.

Setting	PSNR \uparrow	SSIM \uparrow	MAE \downarrow	MSE $_{\text{rel}}\downarrow$
NAFNet	26.21	0.817	0.038	0.049
Concat	26.76	0.826	0.033	0.046
SA	26.59	0.824	0.036	0.047
Concat + SA	26.80	0.829	0.032	0.046
BPA block	26.91	0.831	0.032	0.045

Table 7: Ablation studies of losses.

BPA block	Loss	PSNR \uparrow	SSIM \uparrow	MAE \downarrow	MSE $_{\text{rel}}\downarrow$
\times	$\mathcal{L}_{\text{char}}$	26.21	0.817	0.038	0.049
\times	$\mathcal{L}_{\text{total}}$	26.53	0.822	0.036	0.047
\checkmark	$\mathcal{L}_{\text{char}}$	26.71	0.825	0.034	0.046
\checkmark	$\mathcal{L}_{\text{char}} + \mathcal{L}_{\text{bwl}}$	26.76	0.828	0.033	0.046
\checkmark	$\mathcal{L}_{\text{char}} + \mathcal{L}_{\text{bal}}$	26.81	0.829	0.032	0.046
\checkmark	$\mathcal{L}_{\text{total}}$	26.91	0.831	0.032	0.045

DPD-disp dataset, where the GT disparity is included. We compare with BAMBNet [12] and DPD-disp [15].

First, we consider blur map estimation. To obtain the GT blur map, the pixel with disparity d that satisfies $|d| \leq 1$ is used as the sharp pixel, reversely, it is a blurred pixel. Our method, BAMBNet and DPD-disp [12] respectively have 89.8%/70.2%/88.3% accuracy (the higher, the better, details are in the supplementary material), showing the effectiveness of our method.

Second, we explore disparity estimation. The logits of our unnormalized blurred map are potentially linearly correlated with the ground-truth disparity. Therefore, we compare with the state-of-the-art DP disparity estimation method, DPD-disp [15]. Following [15], we use AI(1), AI(2), and $1 - |\rho_s|$ as the evaluation metrics (the lower, the better). The AI(1), AI(2), and $1 - |\rho_s|$ of our method, BAMBNet, and DPD-disp are 0.063/0.106/0.069, 0.130/0.184/0.096, 0.306/0.772/0.0159. Though our blur map is estimated with a single forward pass, we still achieve

a reasonable performance in the disparity estimation. This potentially explains the high performance of our DP defocus deblurring network, as obtaining the disparity prior benefits the defocus task.

Limitation. As the image encoder of CLIP is trained under a classification-alike pre-training task, it will focus more on local details that help identify its scene class. Textureless regions would produce non-significant semantic reactions, *e.g.*, large areas of wall, ceiling, or floor, and reduce the quality of the estimated blur map. It is possible to use a vision language framework that drives more sensitivity to regions with less texture.

More. In the supplementary material, more qualitative and quantitative evaluations, ablation studies, and analysis are provided.

5. Conclusion and Broader Impact

In this paper, we study end-to-end defocus deblurring of DP images, leveraging the blur-related prior knowledge from the CLIP. We first estimate a blur map with an ensemble of blur-aware and DP-aware strategies, and then use the estimated blur map as the deblurring kernel prior to restoring the DP image. We also propose a blur-aware and blur-weighting loss to regularize the restorations of the DP images during training, by distilling the knowledge of blur from CLIP. In extensive experiments, our method outperforms past works by a large margin in both restoration performance and computation costs.

Broader Impact. The proposed DP-aware strategy is promising to apply and extend CLIP to diverse zero-short stereo vision tasks. We hope it will motivate future work.

Acknowledgment. The work was supported in part by the Beijing Institute of Technology Research Fund Program for Young Scholars, and MiaoMiao Liu was supported by the ARC fellowship and Discovery Project grant (DE180100628, DP200102274).

References

- [1] Abdullah Abuolaim, Mahmoud Afifi, and Michael S Brown. Improving single-image defocus deblurring: How dual-pixel images help through multi-task learning. In *Proceedings of the IEEE/CVF Winter Conference on Applications of Computer Vision*, pages 1231–1239, 2022. [1](#), [2](#), [4](#)
- [2] Abdullah Abuolaim and Michael S Brown. Defocus deblurring using dual-pixel data. In *European Conference on Computer Vision*, pages 111–126. Springer, 2020. [1](#), [2](#), [4](#), [6](#), [7](#)
- [3] Abdullah Abuolaim, Mauricio Delbracio, Damien Kelly, Michael S Brown, and Peyman Milanfar. Learning to reduce defocus blur by realistically modeling dual-pixel data. In *Proceedings of the IEEE/CVF International Conference on Computer Vision*, pages 2289–2298, 2021. [1](#), [2](#), [3](#), [6](#), [7](#)
- [4] Liangyu Chen, Xiaojie Chu, Xiangyu Zhang, and Jian Sun. Simple baselines for image restoration. In *Computer Vision–ECCV 2022: 17th European Conference, Tel Aviv, Israel, October 23–27, 2022, Proceedings, Part VII*, pages 17–33. Springer, 2022. [5](#), [7](#)
- [5] Jia Deng, Wei Dong, Richard Socher, Li-Jia Li, Kai Li, and Li Fei-Fei. Imagenet: A large-scale hierarchical image database. In *2009 IEEE conference on computer vision and pattern recognition*, pages 248–255. IEEE, 2009. [2](#)
- [6] Alexey Dosovitskiy, Lucas Beyer, Alexander Kolesnikov, Dirk Weissenborn, Xiaohua Zhai, Thomas Unterthiner, Mostafa Dehghani, Matthias Minderer, Georg Heigold, Sylvain Gelly, et al. An image is worth 16x16 words: Transformers for image recognition at scale. In *International Conference on Learning Representations*, 2021. [2](#), [6](#), [7](#)
- [7] Rahul Garg, Neal Wadhwa, Sameer Ansari, and Jonathan T Barron. Learning single camera depth estimation using dual-pixels. In *Proceedings of the IEEE/CVF International Conference on Computer Vision*, pages 7628–7637, 2019. [1](#), [3](#)
- [8] Ali Karaali and Claudio Rosito Jung. Edge-based defocus blur estimation with adaptive scale selection. *IEEE Transactions on Image Processing*, 27(3):1126–1137, 2017. [6](#)
- [9] Junyong Lee, Sungkil Lee, Sunghyun Cho, and Seungyong Lee. Deep defocus map estimation using domain adaptation. In *Proceedings of the IEEE/CVF Conference on Computer Vision and Pattern Recognition*, pages 12222–12230, 2019. [6](#)
- [10] Junyong Lee, Hyeongseok Son, Jaesung Rim, Sunghyun Cho, and Seungyong Lee. Iterative filter adaptive network for single image defocus deblurring. In *Proceedings of the IEEE/CVF Conference on Computer Vision and Pattern Recognition*, pages 2034–2042, 2021. [1](#), [2](#), [6](#), [7](#)
- [11] Yu Li, Yaling Yi, Dongwei Ren, Qince Li, and Wangmeng Zuo. Learning dual-pixel alignment for defocus deblurring. *arXiv preprint arXiv:2204.12105*, 2022. [2](#)
- [12] Pengwei Liang, Junjun Jiang, Xianming Liu, and Jiayi Ma. Bambnet: A blur-aware multi-branch network for dual-pixel defocus deblurring. *IEEE/CAA Journal of Automatica Sinica*, 9(5):878–892, 2022. [1](#), [2](#), [6](#), [8](#)
- [13] Xintian Mao, Yiming Liu, Fengze Liu, Qingli Li, Wei Shen, and Yan Wang. Intriguing findings of frequency selection for image deblurring. In *Proceedings of the 37th AAAI Conference on Artificial Intelligence*, 2023. [6](#), [7](#)
- [14] Liyuan Pan, Shah Chowdhury, Richard Hartley, Miaomiao Liu, Hongguang Zhang, and Hongdong Li. Dual pixel exploration: Simultaneous depth estimation and image restoration. In *Proceedings of the IEEE/CVF Conference on Computer Vision and Pattern Recognition*, pages 4340–4349, 2021. [1](#), [2](#), [3](#), [6](#), [7](#)
- [15] Abhijith Punnappurath, Abdullah Abuolaim, Mahmoud Afifi, and Michael S Brown. Modeling defocus-disparity in dual-pixel sensors. In *2020 IEEE International Conference on Computational Photography (ICCP)*, pages 1–12. IEEE, 2020. [1](#), [2](#), [3](#), [4](#), [6](#), [8](#)
- [16] Alec Radford, Jong Wook Kim, Chris Hallacy, Aditya Ramesh, Gabriel Goh, Sandhini Agarwal, Girish Sastry, Amanda Askell, Pamela Mishkin, Jack Clark, et al. Learning transferable visual models from natural language supervision. In *International conference on machine learning*, pages 8748–8763. PMLR, 2021. [1](#), [2](#), [3](#), [6](#)
- [17] Yongming Rao, Wenliang Zhao, Guangyi Chen, Yansong Tang, Zheng Zhu, Guan Huang, Jie Zhou, and Jiwen Lu. Denseclip: Language-guided dense prediction with context-aware prompting. In *Proceedings of the IEEE/CVF Conference on Computer Vision and Pattern Recognition*, pages 18082–18091, 2022. [1](#), [2](#)
- [18] Hyeongseok Son, Junyong Lee, Sunghyun Cho, and Seungyong Lee. Single image defocus deblurring using kernel-sharing parallel atrous convolutions. In *2021 IEEE/CVF International Conference on Computer Vision, ICCV 2021, Montreal, QC, Canada, October 10–17, 2021*, pages 2622–2630. IEEE, 2021. [1](#), [2](#)
- [19] Shumian Xin, Neal Wadhwa, Tianfan Xue, Jonathan T Barron, Pratul P Srinivasan, Jiawen Chen, Ioannis Gkioulekas, and Rahul Garg. Defocus map estimation and deblurring from a single dual-pixel image. In *Proceedings of the IEEE/CVF International Conference on Computer Vision*, pages 2228–2238, 2021. [1](#), [2](#), [3](#), [6](#)
- [20] Yan Yang, Liyuan Pan, Liu Liu, and Miaomiao Liu. K3dn: Disparity-aware kernel estimation for dual-pixel defocus deblurring. In *Proceedings of the IEEE/CVF Conference on Computer Vision and Pattern Recognition (CVPR)*, pages 13263–13272, June 2023. [1](#)
- [21] Syed Waqas Zamir, Aditya Arora, Salman Khan, Munawar Hayat, Fahad Shahbaz Khan, and Ming-Hsuan Yang. Restormer: Efficient transformer for high-resolution image restoration. In *Proceedings of the IEEE/CVF Conference on Computer Vision and Pattern Recognition*, pages 5728–5739, 2022. [2](#), [5](#), [6](#), [7](#)
- [22] Renrui Zhang, Ziyu Guo, Wei Zhang, Kunchang Li, Xupeng Miao, Bin Cui, Yu Qiao, Peng Gao, and Hongsheng Li. Pointclip: Point cloud understanding by clip. In *Proceedings of the IEEE/CVF Conference on Computer Vision and Pattern Recognition*, pages 8552–8562, 2022. [1](#), [2](#)
- [23] Renrui Zhang, Ziyao Zeng, Ziyu Guo, and Yafeng Li. Can language understand depth? In *Proceedings of the 30th ACM International Conference on Multimedia*, pages 6868–6874, 2022. [2](#), [3](#)